Journal of Electronic Science and Technology 24 (2026) 100368

Contents lists available at ScienceDirect

Journal of Electronic Science and Technology

journal homepage: www.keaipublishing.com/en/journals/journal-of-electronic-science-and-technology/



Performance analysis of conventional FR4 antenna prototype and polyimide wearable antenna for ultrawide-band applications

Kondalu Banavathu[a,*], Dattatreya Gopi[b], Krishna Dharavathu[c], Vedula V.S.S.S. Chakravarthy[d], Sujatha Mandala[e], Ahmed Jamal Abdullah Al-Gburi[f,*]

[a] *Department of Electronics and Communication Engineering, NRI Institute of Technology, Vijayawada, 521212, India*
[b] *Department of Electronics and Communication Engineering, Raghu Engineering College, Visakhapatnam, 531162, India*
[c] *National Skill Training Institute, Ministry of Skill Development & Entrepreneurship, Hyderabad, 500013, India*
[d] *Department of Computer Science and Engineering, Vignan's Institute of Information Technology, Visakhapatnam, 530049, India*
[e] *Department of Electronics and Communication Engineering, Lendi Institute of Engineering and Technology, Vizianagaram, 535005,India*
[f] *Strategic Research Institute, Asia Pacific University, Kuala Lumpur, 57000, Malaysia*

ARTICLE INFO

Publishing editor: Yan Wang

Keywords:
Bending
Coplanar waveguide (CPW)
Elliptical monopole
Polyimide (PI)
Ultra-wideband (UWB)
Wearable antennas

ABSTRACT

The rapid advancement of the ultra-wideband (UWB) technology has driven the demand for high-performance antennas with compact size, flexibility, and efficient radiation characteristics. This paper presents a comparative performance analysis of a conventional flame retardant (FR4)-based antenna prototype and a polyimide (PI)-based wearable antenna designed for UWB applications. The antennas are fabricated and evaluated in terms of key performance metrics, including reflection coefficient, impedance bandwidth, gain, and radiation pattern, for wearable applications. The results demonstrate that the FR4-based antenna exhibits stable performance and ease of fabrication, and offers superior flexibility, conformability, and reduced weight, making it highly suitable for body-worn applications. Furthermore, the wearable antenna maintains a wide impedance bandwidth with compactness. These findings provide valuable insights into the trade-offs between rigid and flexible antenna materials, highlighting the potential of PI substrates for the next-generation UWB wearable communication systems.

* Corresponding author.
E-mail addresses: kondalu.phd@gmail.com (K. Banavathu), dattatreya.gopi@gmail.com (D. Gopi), krishnadharavath4u@gmail.com (K. Dharavathu), sameervedula@gmail.com (V.V.S.S.S. Chakravarthy), sujatha.m@lendi.edu.in (S. Mandala), ahmedjamal@ieee.org (A.J.A. Al-Gburi).

https://doi.org/10.1016/j.jnlest.2026.100368
Received 18 May 2025; Received in revised form 8 May 2026; Accepted 13 July 2026; Available online 27 August 2026.
1674-862X/© 2026 The Authors. Publishing Services provided by Elsevier B.V. on behalf of KeAi Communications Co. Ltd. This is an open access article under the CC BY license (http://creativecommons.org/licenses/by/4.0/).

1 Introduction

With the development of new technologies, the demand for larger data rates has increased. The ultra-wideband (UWB) wireless equipment operating at frequencies ranging from 3.1 GHz to 10.6 GHz has already been permitted by the Federal Communications Commission (FCC). Recently, microstrip patch antennas have become increasingly popular because of their minimal price, low density, sporty flat configuration, and ability to conform to the surface of the device. To serve an ever-growing network of users, communication technologies, both fixed and portable, must be dramatically improved.

In recent years, wireless technology networks have undergone tremendous transformation. As a result, both short- and long-term communications are in high demand. A substantial amount of bandwidth is required to cover all wireless services and mobile connectivity. To accomplish this, a low-profile wideband or UWB antenna can be employed [1]. The FCC-approved operating bandwidth and spectrum coverage must be considered in the design and development of UWB antennas. In Ref. [2], a UWB antenna was designed within a range of 3.42–11.70 GHz. A variety of UWB antennas and their designs, approaches, contributions, and performances have been evaluated. In Refs. [3,4], a wideband antenna developed with 3 cm × 3.5 cm × 0.09 cm substrate. A 0.18-cm thin strip line was inserted to improve the resonance frequency between the supplied line and circumferential resonator [5]. A defective ground structure (DGS) refers to the slots on the ground plane of microwave planar circuits. DGS, a new technology, can improve the narrow bandwidth, cross-polarization, and low gain [6]. DGS is a straightforward configuration that improves antenna performance while reducing the cross-formalized radiation from microstrip patches [7]. Therefore, a defectively grounded microstrip antenna is recommended for UWB wireless applications. Three new-style patch antennas, each with a semi-ground plane fed by a microstrip line, were developed and tested. The antenna's impedance bandwidth has been increased from 1.2 GHz to 24.5 GHz, allowing it to cover the S, C, X, Ku, and partially K bands [8]. A lotus-shaped antenna is used for Bluetooth and UWB dual-band functioning, and a sawtooth-shaped defective DGS is used to produce wideband characteristics [9,10]. A coplanar waveguide (CPW)-fed flexible elliptical UWB antenna with multiband elimination is achieved using two circular split-ring resonators (SRRs) with partial ground structures (PGSs) [11]. A tiny flexible antenna with an ultrathin polyimide (PI) substrate was proposed, which can be bent in a specific way to cover the UWB band while maintaining its high levels [12]. In Ref. [13], a round polygonal asymmetrical antenna was designed with polygonal slots organized in a structured area. However, it lacks coverage for most major wireless applications such as industrial, scientific, medical, and WLAN. According to the literature, geometric shapes, electronic band gap (EBG) structures, and antenna systems are employed in the design of transceiver antennas. The UWB antennas can be configured in various ways. A simple CPW with a frequency range of 3.15–32.00 GHz and a −10-dB sensitivity is described [14]. In Ref. [15], UWB antennas on textile materials were examined in terms of their performance and technology. Elliptical-shaped UWB antennas can be stretched, folded, and employed in various ways [16]. Consequently, the flexibility, thermal endurance, and low dielectric loss of the microstrip patch antenna have been highlighted because of its flexible PI substrate [17–23]. In recent work [24], a flexible PI-based quad-port MIMO antenna for wideband sub-6-GHz 5G applications was presented. The proposed antenna employed CPW-fed nested-ring radiators integrated with an X-shaped decoupling structure to achieve wide impedance bandwidth from 2.32 GHz to 7.28 GHz. The design demonstrated stable bending performance, high radiation efficiency of 82%, low envelope correlation coefficient (ECC) (< 0.003), and isolation better than 15.4 dB, making it suitable for wearable and flexible 5G/IoT systems. In addition, the antenna maintained stable operation under conformal bending conditions of up to 45°, while all performance metrics remained within acceptable limits [25–30].

In this study, flame retardant (FR4) and PI-based antenna prototypes were designed for UWB applications. The antennas were fabricated and evaluated for the antenna parameters for both planar and bent characteristics. Additional information regarding the substrate and antenna design is provided in Section 2. Section 3 discusses the implications of the simulations and the results. Finally, Section 4 draws the conclusions.

2 Antenna design and analysis

2.1 Influence of substrate choice and dielectric constant

PI is the optimal substrate choice for increased bandwidth, resonating frequency, and return loss. The thickness of the substrate influences the radiation parameters of the UWB antenna [16]. A thick substrate can be used to increase the efficiency. When low-dielectric-constant substrates are utilized, the omnidirectional RF bandwidth increases. The dielectric properties of the substrates are listed in Table 1.

Table 1
Dielectric constants of substrates.

Material	Dielectric constant
FR4	4.3
Teflon	2.1
Quartz	3.78
Polystyrene	2.6
Nel-tech	3
PI	3.5

Among the investigated substrate materials, PI is considered a suitable choice due to its excellent flexibility and biocompatibility. In addition, PI provides a balanced combination of mechanical stability and electromagnetic performance, making it highly suitable for precise and flexible antenna designs. On the other hand, FR4, with a dielectric constant of 4.3, demonstrated excellent return loss characteristics, indicating low signal reflection. However, its relatively limited bandwidth at higher frequencies restricts its applicability in broadband and high-speed communication systems. Therefore, FR4 is more suitable for low-cost and low-frequency antenna applications. The design methodology and measurement procedures are discussed in this section.

2.2 Antenna geometry

The proposed monopole elliptical-shaped patch (MESP) antenna is designed on a PI substrate. The substrate dimensions are length L_1 = 36.7 mm, width W_1 = 33.0 mm, and thickness h = 0.7 mm. The substrate has a relative permittivity ε_r = 3.5 and loss tangent $(\tan\delta)$ of 0.002. The geometry of the proposed antenna is illustrated in Fig. 1.

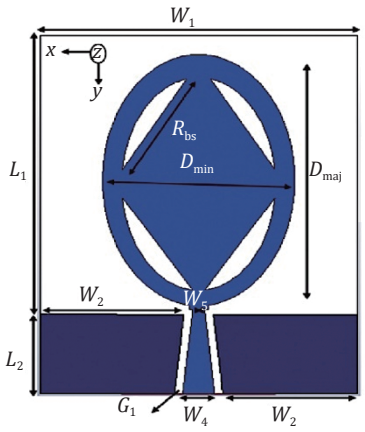


Fig. 1. Geometry of the proposed MESP antenna.

For the FR4 substrate case, the substrate thickness is h = 1.6 mm, the relative permittivity is ε_r = 4.3, and the loss tangent $(\tan\delta)$ is 0.025. The remaining geometrical parameters are defined as follows: L_2 denotes the ground-plane length, W_2 and W_3 represent the ground-plane widths, W_4 is the microstrip feed-line width, W_5 is the feed-gap width, G_1 is the coupling gap, D_{maj} is the major diameter of the elliptical patch, D_{min} is the minor diameter of the elliptical patch, and R_{bs} represents the radius of the bottom circular section. The optimized dimensions are l_2 = 10.30 mm, W_2 = 14.00 mm, W_3 = 14.96 mm, W_4 =3.30 mm, W_5 = 2.00 mm, G_1 = 0.85 mm, D_{maj} = 32.93 mm, D_{min} = 19.97 mm, and R_{bs} = 14.21 mm. The antenna was excited using a 50-Ω microstrip feed line, as depicted in Fig. 1.

The proposed antenna was designed and simulated using CST Microwave Studio, which is based on the finite integration technique (FIT) [17].

A statistical study was conducted to determine how narrowing graduation evolves with time. The variables (defective ground length, emitting unit, and feeding spacing) remained unchanged until the ideal choice was made in the initial situation. The parametric analysis with R_{bs} is shown in Fig. 2(a), and the comparison of the proposed MESP antenna's reflection coefficient (S_{11}) with that of other materials is shown in Fig. 2(b). The optimal spacing resulted in the lowest S_{11}.

The evolutionary design process of the MESP antenna, along with its S_{11} performance, is illustrated in Figs. 3 and 4. The initial designed Antenna 1 (Fig. 3(a)) represents a simple UWB antenna with an elliptical radiating patch and a modified ground plane featuring right and left oblong extensions beside the feed line.

This configuration uses the dimensions (D_{maj} = 32.93 mm, D_{min} = 19.97 mm) and achieves a maximum S_{11} of approximately − 25 dB. The dimensions of the MESP are calculated as follows [25]:

$$f_{Lower} = \frac{7.2}{\left(2D_{maj} + \frac{D_{min}}{4} + l_2\right)\sqrt{\varepsilon_r}} \quad (1)$$

where f_{Lower} is the lower resonant frequency, and l_2 is the ground-plane length.

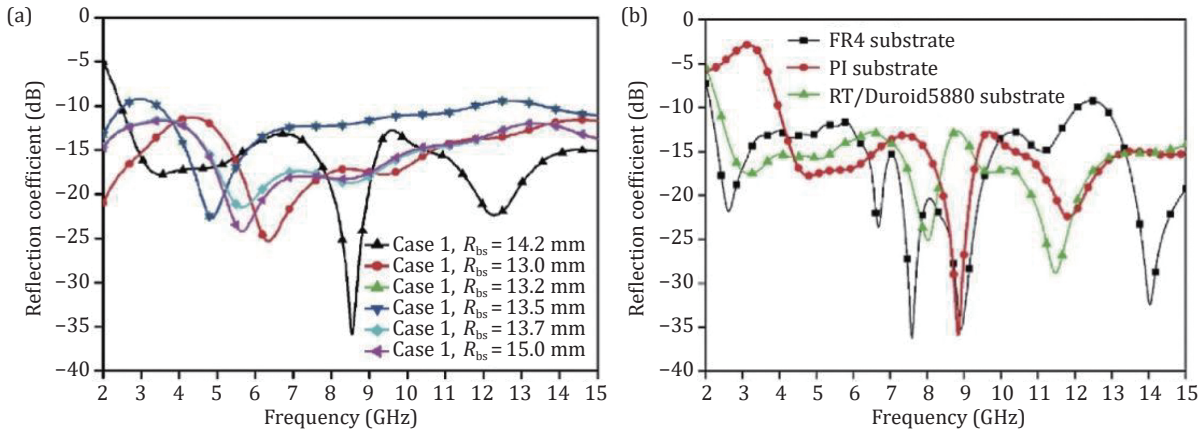


Fig. 2. Parametric and material analysis of the proposed MESP antenna: (a) parametric analysis of the bottom-section radius (R_{bs}) and (b) comparison of the reflection coefficient (S_{11}) for different substrate materials.

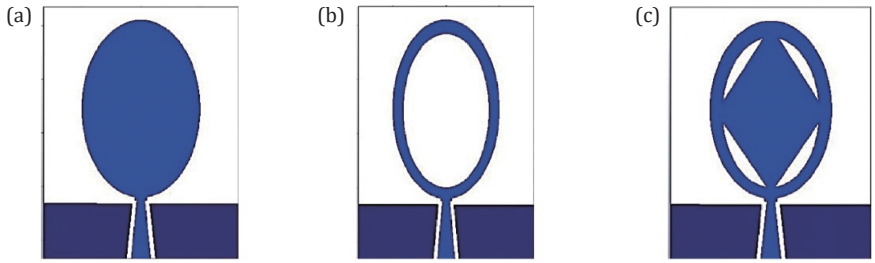


Fig. 3. Evolution design process of the MESP antennas: (a) Antenna 1 (circular), (b) Antenna 2 (ring), and (c) Antenna 3 (proposed).

To improve impedance matching and enhance S_{11}, Antenna 2 (Fig. 3(b)) introduces a central elliptical slot (with major and minor radii of 27.86 mm and 16.28 mm, respectively) into the patch. This modification results in a deeper notch with S_{11} of approximately −29 dB. Finally, Antenna 3 (Fig. 3(c)) incorporates four rhombus-shaped slots into the elliptical patch to further broaden the bandwidth and enhance performance. As shown in Fig. 4, this final design achieves a reflection coefficient of −32 dB and offers a wide operational bandwidth ranging from 2.49 GHz to 15.00 GHz, indicating substantial enhancement compared with the previous stages. Table 2 presents a comprehensive assessment of the performance of the MESP antennas.

The equivalent circuit of the MESP antenna is illustrated in Fig. 5(c). The major and minor axes of the elliptical patch affected the impedance bandwidth. The values of each component are R_1 =

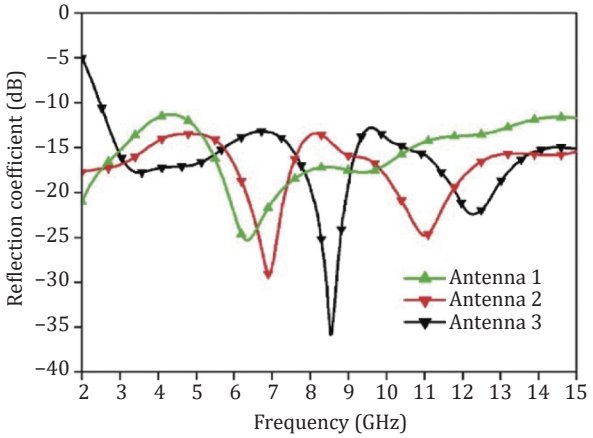


Fig. 4. S_{11} results of the MESP antennas.

3.01 Ω, L_1 = 2.41 nH, L_2 = 5.72 nH, C_1 = 2.830 pF, and C_2 = 0.071 pF.

3 Results and analysis

3.1 Planar state

Photographs of the MESP antenna fabricated using PI and FR4 substrate materials are shown in Fig. 5. Fig. 6 shows the measurement setup for the PI and FR4 substrate materials for the proposed MESP antenna. Fig. 7 shows the simulated S_{11} of the antenna. The antenna's suggested impedance range is indicated in Fig. 7 for a frequency range of 2.49–15.00 GHz. Overall, PI substrate material yielded good results compared with the FR4 substrate material. The test findings matched those of the simulations. Minor variations between the measurements and simulations may occur owing to fabrication errors. However, conflicts cannot be created through simulations. Simulated S_{11} has a bandwidth of 12.51 GHz (2.49–15.00 GHz) and a gain of 6.3 dBi. The rhombus shape increases the bandwidth and gain, while decreasing the resonant frequency. Many wireless applications benefit from this added capacity. WiMAX applications use 3.3–3.8 GHz, WLAN uses 5.15–5.35 GHz, and wireless transmission uses 5.725–5.825 GHz, among other frequencies.

Table 2
Performance evolution of the MESP antennas.

Evolution	Frequency (GHz)	S_{11}	Bandwidth (GHz)	Gain (dBi)
Antenna 1	2.79–10.20	25	7.41	3.20
Antenna 2	2.79–11.10	29	8.31	3.35
Antenna 3	2.49–15.00	32	12.51	6.30

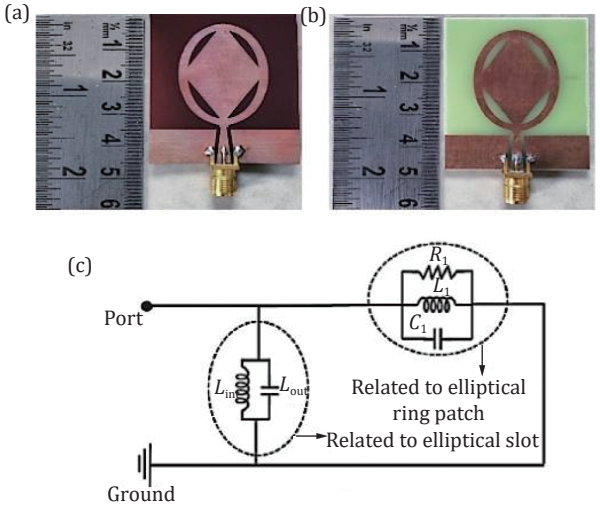


Fig. 5. Fabrication of the MESP antenna with different substrate materials: (a) PI, (b) FR4, and (c) equivalent diagram of the MESP antennas.

Table 3 presents the simulated and measured S_{11} values. Simulated and measured S_{11} results were obtained to validate the agreement. The measured S_{11} bandwidth is 12.60 GHz, while the simulated bandwidth is 12.51 GHz.

There are a few factors to consider when choosing an antenna. The MESP antenna radiation efficiencies of the PI and FR4 substrate materials are shown in Fig. 8. The radiation efficiency of the PI substrate materials was 97.12% at 8.56 GHz. Over the 2.5 GHz to 15.0 GHz band, the efficiencies range from 93.3% to 99.3%. However, PI substrate materials performed better than FR4 substrate materials across the full bandwidth. The radiation efficiency and gains of MESP antennas can be increased by using a lossless microwave substrate. Equation (2) can be used to calculate the antenna gain. The simulated peak gains were observed at 6.15 dBi, as shown in Fig. 9.

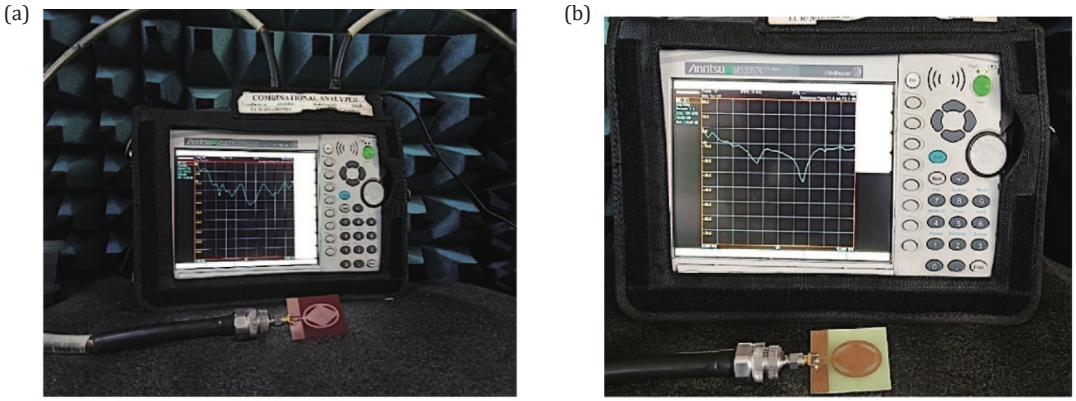


Fig. 6. Measurement setup of the proposed MESP antenna with different substrate materials: (a) PI and (b) FR4.

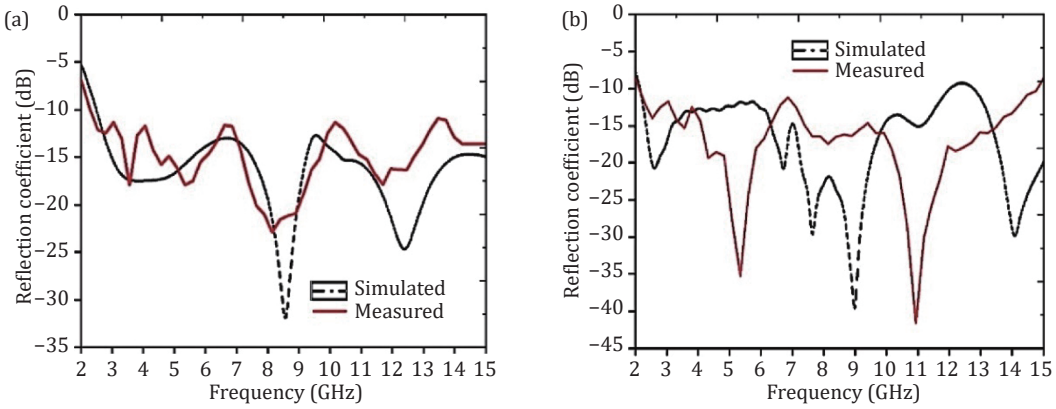


Fig. 7. Simulated and measured S_{11} for MESP antennas with different substrate materials: (a) PI and (b) FR4.

Table 3
Simulated and measured S_{11} results of the MESP antennas.

Measurement	Reflection coefficient S_{11} (dB)	Operating frequency (GHz)	Bandwidth (GHz)
Simulated	−32	2.49–15.00	12.51
Measured	−24	2.40–15.00	12.60

$$G_{\mathrm{AUT}} = G_{\mathrm{Ref}} + 10\lg\left(\frac{P_{\mathrm{AUT}}}{P_{\mathrm{Ref}}}\right) \quad (2)$$

where G_{AUT} is the gain of the antenna under test (AUT) in dBi, G_{Ref} is the gain of the reference antenna in dBi, P_{AUT} is the received power using AUT, and P_{Ref} is the received power using the reference antenna.

Fig. 10 shows how the surface current flows through the antenna's PI and FR4 substrate materials. The substrate patch and feed line are more sensitive to the surface current than the FR4 substrate. According to the current and voltage, the impedance of the PI substrate patch and the edges of the PI substrate material are in close proximity to the feeding line and edges. Fig. 11 shows the proposed antenna for a radiation pattern. Figs. 12(a) and (b) illustrate the normalized 2-dimensional radiation patterns radiated by a modelled MESP antenna in both co- and cross-polarizations, respectively. Fig. 12(a) shows that for the three frequencies, the co-polar is higher than the cross-polar (see Fig. 12 for more information). It is less than 26 dB in the E-plane. The cross-polar magnitude is 36 dB smaller at 0° than the co-polar magnitude in the H-plane at 3.8 GHz. At 3.8 GHz, the radiation was omnidirectional. The 8.56-GHz radiation is still omnidirectional. However, larger harmonics at 8.56 GHz raise the cross-polar values. Again, its magnitude was below 17 dB in the E-plane. At 12.4 GHz, the cross-polar magnitude was 37 dB smaller than the co-polar magnitude at 0°. The planned MESP antenna radiated well in all directions.

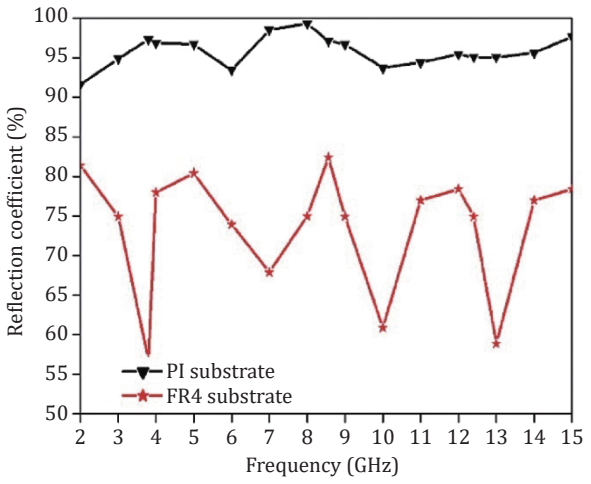


Fig. 8. Radiation efficiency comparison of the proposed MESP antenna with different substrate materials: (a) PI and (b) FR4.

3.2 Bent state

The bending radius of a curved antenna surface has a significant influence on its electromagnetic performance, particularly on its resonant frequency and bandwidth. When an antenna, such as a microstrip

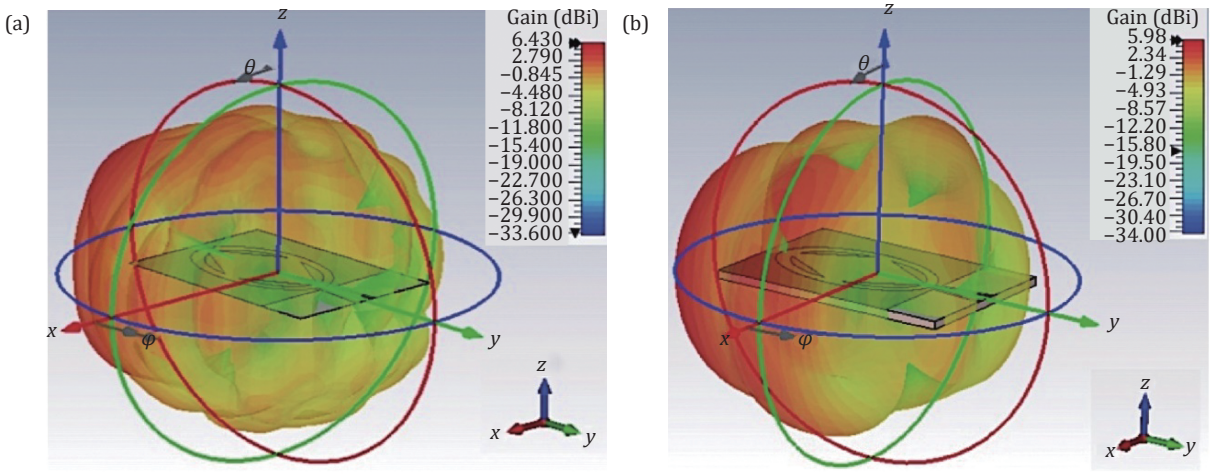


Fig. 9. 3D gain (dBi) of the proposed MESP antenna with different substrate materials: (a) PI and (b) FR4.

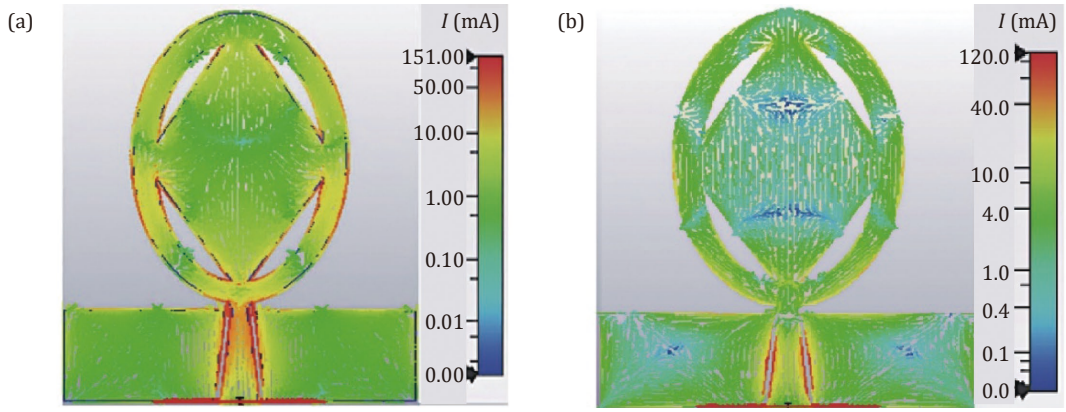


Fig. 10. Surface current distribution of the proposed MESP antenna with different substrate materials: (a) PI and (b) FR4.

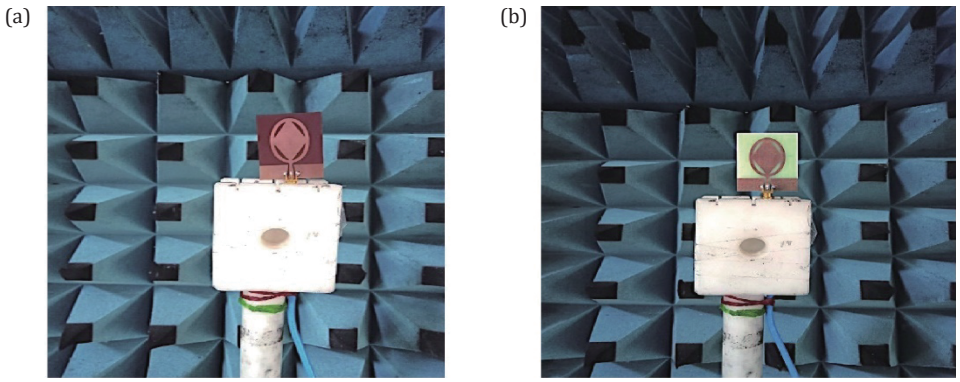


Fig. 11. Radiation pattern measurement setup of the proposed MESP antenna with different substrate materials: (a) PI and (b) FR4.

or patch type, was bent over a curved surface, the geometry and distribution of the surface currents changed, leading to variations in its operating characteristics. For a convex surface with a large bending radius of approximately 47.67 mm, the curvature was relatively gentle. In this case, the patch stretched slightly outward, effectively increasing its electrical length. Consequently, the resonant frequency decreased slightly because it is inversely proportional to the effective length of the radiating element. The bandwidth may also

be reduced marginally owing to a small change in impedance matching, but the overall effect remains moderate because of the large radius.

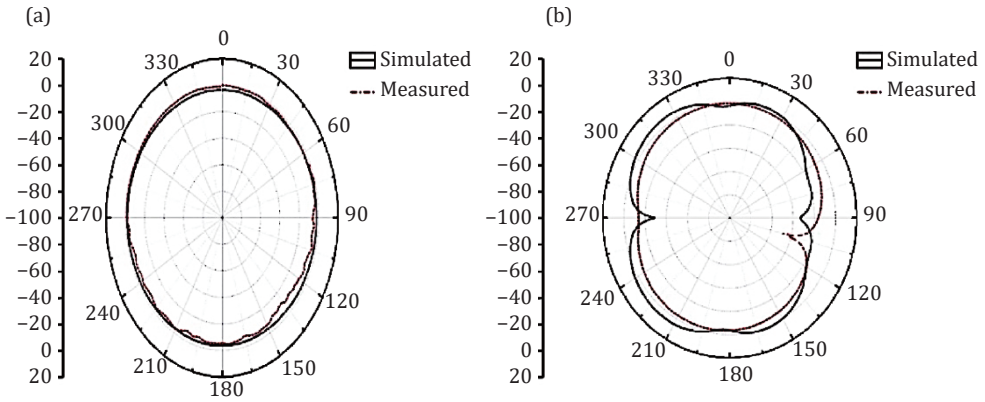


Fig. 12. Radiation pattern characteristics of the proposed MESP antenna: (a) E-plane and (b) H-plane.

By contrast, for a concave surface with a smaller bending radius of approximately 9.52 mm, the antenna surface bent inward, compressing the patch and reducing its effective length. This leads to a noticeable increase in the resonant frequency compared with its flat or convex counterpart. The tighter curvature also causes greater non-uniformity in the field distribution, resulting in a reduced bandwidth, poorer impedance matching, and possible radiation pattern distortion. Generally, as the bending radius decreases, antenna sensitivity increases, indicating that the performance becomes more unstable and susceptible to geometric variations.

Therefore, for conformal or flexible antenna designs, it is recommended to maintain a larger bending radius (preferably greater than five times the patch length) to preserve a stable performance. Among the two cases, convex bending is less detrimental to the antenna characteristics than concave bending because it causes only mild shifts in frequency and limited bandwidth reduction. Overall, the study of the bending radius effects highlights the importance of mechanical flexibility and surface curvature considerations in modern antenna design.

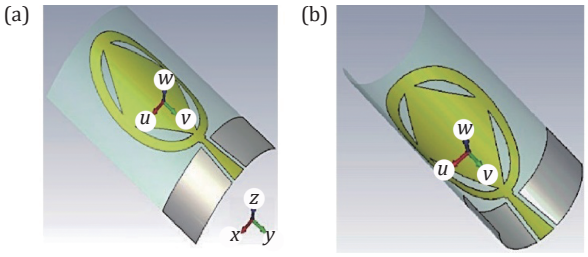


Fig. 13. Simulated bending models of the MESP antennas in bending states: (a) concave and (b) convex.

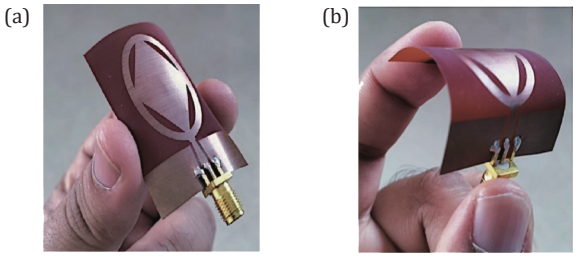


Fig. 14. Fabrication of the MESP antennas under bending conditions: (a) vertical and (b) horizontal.

Fig. 13 shows the simulated models of concave and convex bending of the proposed MESP antenna. Fig. 14 shows the fabricated models with their bending characteristics. The measurement setup is shown in Fig. 15, where S_{11} parameters of the concave and convex conditions are approximately equal to the entire bandwidth pattern, even if the resonance locations are altered significantly. For concave bending, the proposed antenna resonates at an 8.56 GHz frequency with an S_{11} of −32 dB and a bandwidth of 2.49–15 (12.51) GHz, as shown in Fig. 16, antenna gains for concave and convex antennas. According to the results shown in Table 4, the concave antennas have a peak gain of 6.74 dBi. At 7.2-dBi gain, comparable convex bend antennas were discovered. The 3D gain plots are shown in Fig. 17. Stretching changes the resonance of the antenna by altering its actual dimensions. These studies demonstrate that this antenna can withstand a variety of difficult situations, including its close proximity to curved shapes. Fig. 16 shows the simulated and measured S_{11} for bending the MESP antennas.

Fig. 18 shows the surface current distributions of the proposed antenna under concave and convex bending states. At 8.55 GHz, the current distribution was observed at 64.9 A/m. Fig. 18(a) depicts the current distribution at 0°, whereas Fig. 18(b) depicts the current distributions at 180° for the concave bending characteristics. The current intensity varies at different phase angles. Fig. 18(c) depicts the current distribution at 0°, whereas Fig. 18(d) depicts the current distributions at 180° for the convex analysis. The current intensity varies at different phase angles.

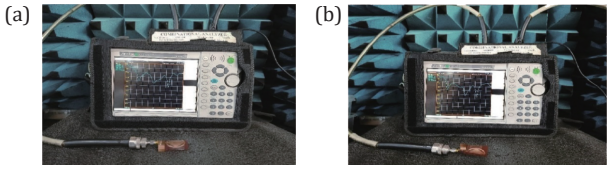


Fig. 15. Measurement setup of the MESP antennas in bending states: (a) concave and (b) convex.

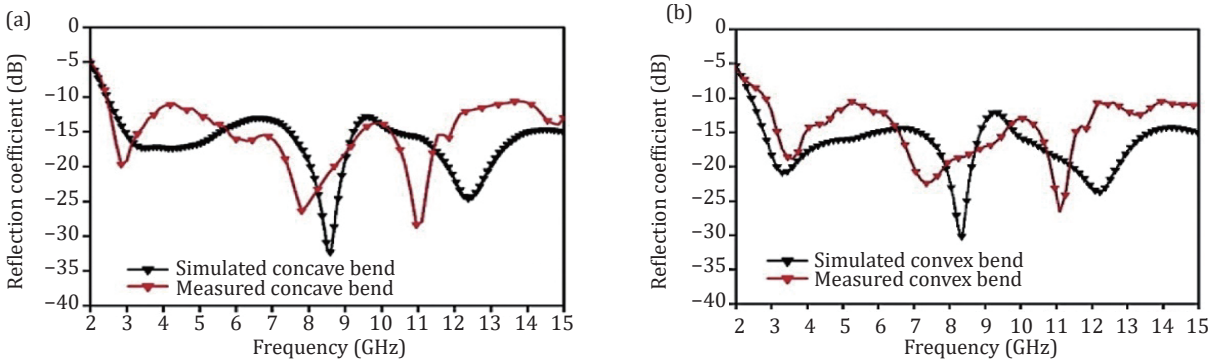


Fig. 16. Simulated and measured S_{11} of the MESP antennas in bending states: (a) concave and (b) convex.

Table 4
Optimized results of the MESP patch antenna.

Antenna	Frequency band in use (GHz)	Broadband (GHz)	Radiation efficiency variation (%)	Gain (dBi)
Planar shape	2.49–15.00	12.510	93.3–99.3	6.30
Concave bend	2.457–15.00	12.543	91.1–98.8	6.74
Convex bend	2.428–15.00	12.572	88.3–98.5	7.20

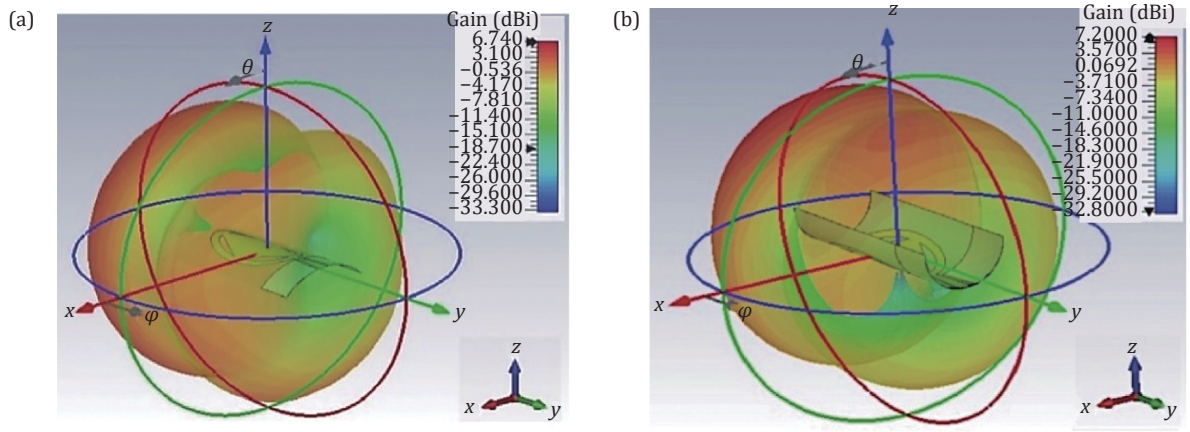


Fig. 17. 3D gain of the MESP antennas in bending states: (a) concave and (b) convex.

Fig. 19(a) shows the E-plane and H-plane patterns for both polarities. For the co-polar, the main lobe magnitude is observed at −0.232 dBi at 0°. For cross-polar, the main lobe magnitude is −10.400 dBi, with the primary lobe at 221.0°. An angle of 3.0 dB was observed at 51.3°, with a lateral lobe level of −0.8 dB. It was observed that the cross-polar magnitude and angular width were reduced compared to the co-polar

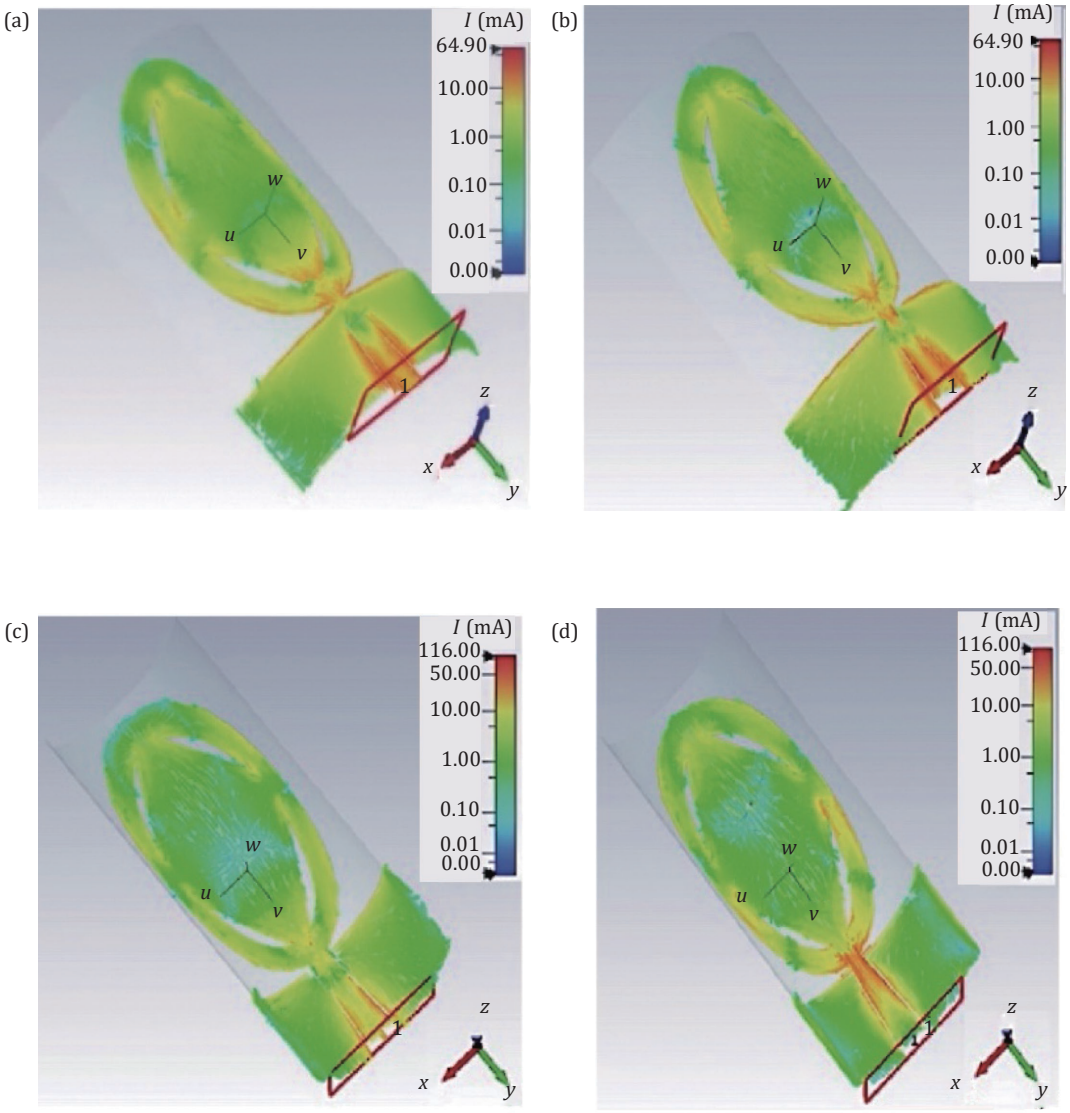


Fig. 18. MESP antenna current distribution of concave bend at (a) 0°, (b) 180°, (c) 0°, and (d) 180°.

magnitude. For H-plane patterns, the co-polar main lobe magnitude is observed at 6.590 dBi at 220.0° with an angular width of 42.6° and a side lobe level of −2.4 dB. For the cross-polar region, the main lobe magnitude was −41.000 dBi, with the primary lobe at 222.0°. An angle of 3.0 dB was observed at 91.2°, with a lateral lobe level of −0.9 dB. Fig. 19(b) depicts the co-polar and cross-polar for both E-plane and H-plane. It is observed that for the co-polar, the main lobe magnitude is observed at −0.689 dBi at 359.0°. An angular width of 83° with a 3.0-dB angular width was observed. For the cross-polar region, the main lobe magnitude was −17.000 dBi with a main lobe direction of 143.0°. At 39.7°, an angular width of 3.0 dB is observed. The co-polar main lobe magnitude is 7.080 dBi at 318.0° with an angular width of 44.4°, while the side lobe level is −4.0 dB. For cross-polar, the main lobe magnitude is −23.600 dBi, with the primary lobe at 277.0°. An angle of 3.0 dB was observed at 72.8°, with a lateral lobe level of −4.60 dB.

Table 5 presents a comparative analysis of the proposed antenna with other relevant antennas. The proposed MESP antenna outperforms the other antennas in terms of area, substrate material, operating frequency, bandwidth, and peak gain. An increased bandwidth can be achieved using elliptical radiating patches with contours or mild curvature. These methods can be used to improve spectra. The DGS construction of the MESP antenna has slots that allow it to receive a wider variety of frequencies while remaining compact.

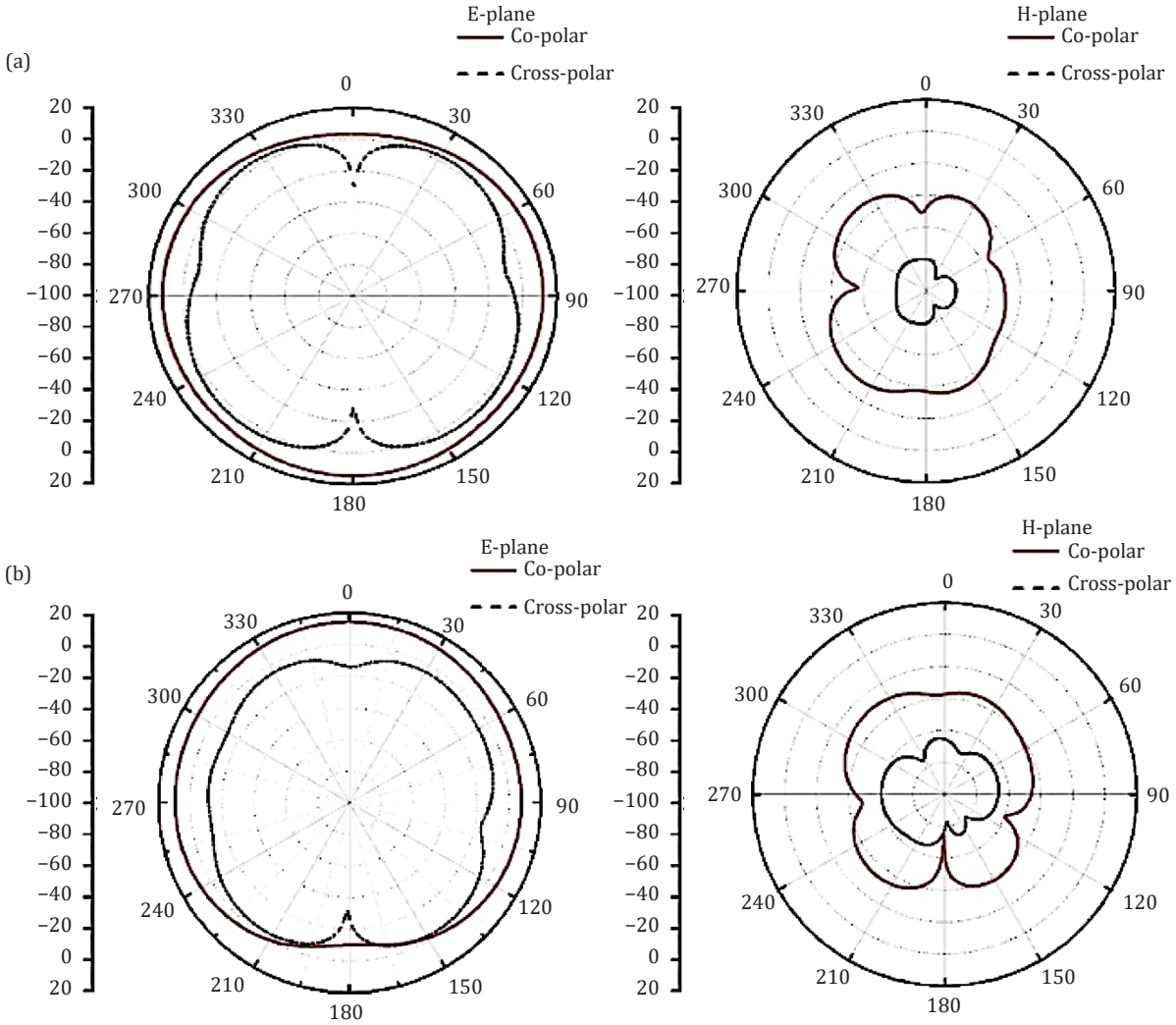


Fig. 19. MESP antenna radiation pattern in bending states: (a) concave and (b) convex.

Table 5
MESP antenna comparisons with various UWB antennas.

Ref.	Size of antenna (mm^3)	Substrate material	Frequency range in use (GHz)	Bandwidth (GHz)	Peak gain (dBi)
[9]	44×42×1.6	FR4	2.60–12.30	8.70	6.20
[10]	30×25×0.8	RT/Duroid5880	3.10–11.50	8.40	5.25
[11]	45×35×0.6	Teflon	1.05–13.00	11.95	5.40
[18]	80×80×1.6	FR4	3.10–10.60	7.50	7.90
[19]	48×34×0.13	PI	1.00–8.00	7.00	3.10
[12]	30.4×38×0.07	PI	3.06–13.50	10.44	5.00
[13]	31×45×1.575	RT/Duroid5870	2.18–44.50	42.32	4.38
[20]	80×80×1.6	FR4	2.40–24.00	21.50	5.00
[21]	33×47×0.0508	PI	2.20–14.30	12.10	4.90
[22]	36×42×1.6	FR4	4.50–13.50	9.00	6.00
[23]	21×22×1.6	FR4	4.00–14.00	10.00	4.33
[24]	46 × 46.5 × 0.6	PI	2.32–7.28	4.96	4.42
Proposed	47×33×0.7	PI	2.49–15.00	12.51	6.30

4 Conclusions

A simple, low-profile MESP was designed and tested for UWB applications on a 47 mm × 33 mm × 0.07 mm Kapton PI substrate. The proposed antenna was compact, easy to fabricate, and occupied minimal space. The design utilized flexible, resilient, and low-dielectric-loss Kapton PI substrates. The bandwidth and gain performance were enhanced using a CPW feed structure integrated into the substrate. A tapered CPW feed line excited the radiating element, resulting in improved impedance matching across the operational frequency range. The MESP achieves an impedance bandwidth of 12.51 GHz and a peak gain of 6.30 dBi, outperforming conventional antennas. The antenna exhibited quasi-omnidirectional radiation patterns in both the E-plane and H-plane. The design was simulated using CST and validated experimentally using a vector network analyzer. Under bending conditions, the antenna demonstrated minimal degradation in impedance matching and radiation characteristics. Owing to its flexibility, reliability, portability, ease of fabrication, and favorable radiation and impedance characteristics, the proposed antenna is well suited for UWB applications.

Acknowledgments

The authors sincerely thank NRI Institute of Technology and the Strategic Research Institute (SRI), Asia Pacific University, for providing the necessary materials and support that made this research successful.

CRediT authorship contribution statement

Kondalu Banavathu: Writing—original draft, Visualization. **Dattatreya Gopi**: Resource, Methodology, Investigation. **Krishna Dharavathu**: Formal analysis. **Vedula V.S.S.S. Chakravarth**y: Writing—review & editing, Methodology, Investigation, Formal analysis. **Sujatha Mandala**: Formal analysis, Validation, Investigation. **Ahmed Jamal Abdullah Al-Gburi**: Conceptualization, Investigation, Resource management, Supervision, Project administration, Funding acquisition.

Declaration of competing interest

The authors declare no conflicts of interest.

References

[1] J. Chen, F. Yang, S.-J. Zhao, et al., Airborne ultra-low profile ultra-wideband omnidirectional antenna based on tightly coupled arrays, Journal of Electronic Science and Technology 22 (4) (2024) 100289.
[2] N.M. Awad, M.K. Abdelazeez, Multislot microstrip antenna for ultra-wide band applications, Journal of King Saud University-Engineering Sciences 30 (1) (2018) 38–45.
[3] A. Sid, P.-Y. Cresson, N. Joly, et al., Bio-based substrate for flexible electronics——application to a 2.45 GHz wearable patch antenna, Mater. Today Electron. 5 (2023) 100049.
[4] D. Nagar, P. Ranjan, A. Chowdhury, Flexible metasurface loaded felt substrate built wearable antenna with tri-band and high gain features for WBAN applications, J. Electron. Mater. 54 (7) (2025) 5918–5927.
[5] S. Baudha, K. Kapoor, M.V. Yadav, U-shaped microstrip patch antenna with partial ground plane for mobile satellite services (MSS), in: Proc. of URSI Asia-Pacific Radio Science Conf., New Delhi, India, 2019, pp. 1–5.
[6] M.K. Khandelwal, B.K. Kanaujia, S. Kumar, Defected ground structure: fundamentals, analysis, and applications in modern wireless trends, Int. J. Antenn. Propag. 2017 (2017) 2018527.
[7] Y.-F. Mao, S.-T. Guo, M.-G. Chen, Compact dual-band monopole antenna with defected ground plane for Internet of things, IET Microw. Antenna. P. 12 (8) (2018) 1332–1338.
[8] M.K. Khandelwal, Analysis of frequency notch characteristics in enhanced-ultra-wide-band compact microstrip patch antenna, Wireless Pers. Commun. 100 (3) (2018) 1249–1260.
[9] M. Samsuzzaman, M.Z. Mahmud, M.T. Islam, et al., Compact lotus shape dual band patch antenna for Bluetooth and ultra wideband applications, Microw. Opt. Techn. Let. 59 (7) (2017) 1590–1597.
[10] B.P. Nadh, B.T.P. Madhav, M.S. Kumar, et al., Circular ring structured ultra-wideband antenna for wearable applications, Int. J. RF Microw. C. E. 29 (4) (2019) e21580.
[11] S. Lakrit, S. Das, S. Ghosh, et al., Compact UWB flexible elliptical CPW-fed antenna with triple notch bands for wireless communications, Int. J. RF Microw. C. E. 30 (7) (2020) e22201.
[12] Y. Zhang, S.-D. Li, Z.-Q. Yang, et al., A coplanar waveguide-fed flexible antenna for ultra-wideband applications, Int. J. RF Microw. C. E. 30 (8) (2020) e22258.

[13] M.A. Dorostkar, M.T. Islam, R. Azim, Design of a novel super wide band circular-hexagonal fractal antenna, Prog. Electromagn. Res. 139 (2013) 229–245.
[14] S. Hakimi, S.K.A. Rahim, M. Abedian, et al., CPW-fed transparent antenna for extended ultrawideband applications, IEEE Antenn. Wirel. Pr. 13 (2014) 1251–1254.
[15] M.S. Mahmud, S. Dey, Design and performance analysis of a compact and conformal super wide band textile antenna for wearable body area applications, in: Proc. of 6th European Conf. on Antennas and Propagation (EUCAP), Prague, Czech Republic, 2012, pp. 1–5.
[16] A.J.A. Al-Gburi, Z. Zakaria, M. Palandoken, et al., Super compact UWB monopole antenna for small IoT devices, Comput. Mater. Con. 73 (2) (2022) 2785–2799.
[17] P. Kumar, A.K. Singh, R. Kumar, et al., High isolated defected ground structure based elliptical shape dual element MIMO antenna for S-band applications, Progress in Electromagnetics Research C 143 (2024) 67–74.
[18] Ö. Küçüksarı, S. Çimen, G. Çakır, Constant gain modified antipodal Vivaldi antenna with rake-like wires operating over 3.1–10.6 GHz, Microw. Opt. Techn. Let. 60 (5) (2018) 1205–1211.
[19] Z. Hamouda, J.-L. Wojkiewicz, A.A. Pud, et al., Flexible UWB organic antenna for wearable technologies application, IET Microw. Antenna. P. 12 (2) (2018) 160–166.
[20] D.-Q. Yang, J.-Z. Hu, S.-H. Liu, A low profile UWB antenna for WBAN applications, IEEE Access 6 (2018) 25214–25219.
[21] H.R. Khaleel, H.M. Al-Rizzo, D.G. Rucker, et al., A compact polyimide-based UWB antenna for flexible electronics, IEEE Antenn. Wirel. Pr. 11 (2012) 564–567.
[22] A. Sharma, P. Khanna, K. Shinghal, et al., Design of CPW-fed antenna with defected substrate for wideband applications, J. Electr. Comput. Eng. 2016 (2016) 6546481.
[23] R.G. Mishra, R. Mishra, P. Kuchhal, et al., Design and analysis of CPW-fed microstrip patch antennas for wide band applications, in: Proc. of the Intl. Conf. on Inventive Computing and Informatics, Coimbatore, India, 2017, pp. 651–654.
[24] P. Okas, A. Sharma, R.K. Gangwar, Super-wideband CPW fed modified square monopole antenna with stabilized radiation characteristics, Microw. Opt. Techn. Let. 60 (3) (2018) 568–575.
[25] V.N.K.R. Devana, A.K. Sohi, A. Swetha, et al., Assessment of a flexible polyimide-based quad-port MIMO antenna for wideband sub-6 GHz 5G applications, Ain Shams Eng. J. 17 (5) (2026) 104044.
[26] A.J.A. Al-Gburi, N.H.M. Radi, T. Saeidi, et al., Superconductive and flexible antenna based on a tri-nanocomposite of graphene nanoplatelets, silver, and copper for wearable electronic devices, J. Sci.-Adv. Mater. Dev. 9 (3) (2024) 100773.
[27] M.S. Yahya, U. Musa, M.S. Zidan, et al., Machine learning-optimized compact dual-band medical syringe-inspired wearable antenna for efficient WBAN applications, Sci. Rep.-UK 15 (1) (2025) 43240.
[28] A.J.A. Al-Gburi, M.M. Ismail, N.J. Mohammed, et al., SAR flexible antenna advancements: highly conductive polymer-graphene oxide-silver nanocomposites, Prog. Electroma. Res. M 127 (2024) 23–30.
[29] G. Singla, R. Sharma, R. Khanna, et al., Design of a flexible, highly isolated multiband f-meta MIMO antenna for 5G sub-6 GHz applications using the theory of characteristic modes, Optik 345 (2026) 172632.
[30] A.J.A. Al-Gburi, N.J. Mohammed, T. Saeidi, et al., Design and development of a graphene-based MIMO antenna for smart multi-band sub-6 GHz 5G wearable communication applications, Sci. Rep.-UK 16 (1) (2026) 12873.



Kondalu Banavathu is currently a Professor with NRI Institute of Technology (NRIIT), Vijayawada, India, with over 17 years of teaching and research experience in electronics and communication engineering. His research interests include conformal antenna, multiple-input multiple-output (MIMO) antenna, antennas for 5G/6G, and IoT.



Dattatreya Gopi received the B.Tech. degree in electronics and communication engineering from Jawaharlal Nehru Technological University, Kakinada, India in 2009, the M.Tech. degree in radar and microwave engineering from Andhra University College of Engineering, Visakhapatnam, India in 2014, and the Ph.D. degree in the field of antennas from KL University, Guntur, India in 2020. He is currently affiliated with Raghu Engineering College, Vijayawada, India. His current research interests include testability of design, flexible antennas, concentric circular ring antennas, conformal antennas, biomedical antennas, and textile antennas.



Krishna Dharavathu is a Training Officer at the National Skill Training Institute (NSTI), Hyderabad, India with over 18 years of teaching and research experience in electronics and communication engineering. His research interests include wireless communication, MIMO systems, image encryption, antennas for 5G/6G, VLSI, IoT, and AI-based engineering applications.



Vedula V.S.S.S. Chakravarthy is currently a Professor with the Department of Computer Science and Engineering, Vignan's Institute of Information Technology, Visakhapatnam, India. He is the Chair of IEEE Vizag Bay ComSoc/SPS Joint Chapter and Treasurer in Wireless, Antenna, and Microwave Symposium Society. He is the Fellow of Institute of Electronics and Telecommunication Engineers (IETE), Senior Member of IEEE, and Life Senior Member of Wireless, Antenna, and Microwave Symposium Society (WAMS), and Member of Applied Computational Electromagnetics Society (ACES), Life Member of Soft Computing Research Society (SCRS), and several other professional bodies. His research interests include computational electromagnetics and antennas as well as soft-computing and evolutionary computing tools.



Sujatha Mandala received the M.Tech. dgree from Jawaharlal Nehru Technological University, Kakinada, India in 2012, and the B.E. degree from Andhra University, Visakhapatnam, India in 2008. She is currently pursuing the Ph.D. degree in antennas with electromagnetic soft surface (EMSS), Lendi Institute of Engineering and Technology, Vizianagaram, India, where she is also an Assistant Professor. Her research interests include microwave, radio frequency, and antenna design. She has published more than 20 papers in reputed SCI and Scopus indexed journals.



Ahmed Jamal Abdullah Al-Gburi (Senior Member, IEEE) received the M.Eng. and Ph.D. degrees in electronics and computer engineering (telecommunication systems) from Universiti Teknikal Malaysia Melaka, Malacca, Malaysia in 2017 and 2021, respectively. He is currently an Associate Professor with the Strategic Research Institute (SRI), Asia Pacific University (APU), Kuala Lumpur, Malaysia. Previously, he served as a Senior Lecturer and Deputy Head of the Microwave Research Group (MRG), Center for Telecommunication Research and Innovation (CeTRI), Universiti Teknikal Malaysia Melaka. His research interests include microwave sensors, metasurfaces, metamaterials, and MIMO antennas. He has authored numerous journal and conference publications and received several awards in innovation competitions. He is also a registered member of Board of Engineers Malaysia (BEM), Malaysia Board of Technologists (MBOT), and International Association of Engineers (IAENG). In 2023, 2024, and 2025, he was recognized among the World's Top 2% Scientists by Stanford University, published by Elsevier.